EURASIP Journal on Advances in Signal Processing

RESEARCH Open Access

Low-complexity selective mapping technique for PAPR reduction in downlink power domain OFDM-NOMA

Mohamed Mounir[1,2*], Mohamed Ibrahim Youssef[1] and Ashraf Mohamed Aboshosha[3]

*Correspondence: MohamedMounir.2214@azhar.edu.eg

[1] Department of Electrical Engineering, Faculty of Engineering, Al-Azhar University, Cairo, Egypt
[2] Department of Electronics and Communications Engineering, El Gazeera High Institute for Engineering and Technology, Cairo, Egypt
[3] NCRRT, Egyptian Atomic Energy Authority, Cairo, Egypt

Abstract

To support ultra-massive connectivity, non-orthogonal multiple access (NOMA) techniques are expected to be used in 6G instead of conventional orthogonal multiple access (OMA) techniques. Furthermore, given that orthogonal frequency division multiplexing (OFDM) was used by 4G and 5G, NOMA is expected to be combined with OFDM to mitigate frequency selectivity in multipath channels. However, after passing through nonlinear high power amplifiers (HPAs), OFDM-NOMA has reportedly suffered from nonlinear distortion due to the high peak-to-average power ratio (PAPR) problem, thus reducing users' achievable data rates, sum rate capacity, and users' bit error rate after going through nonlinear HPAs. Many PAPR reduction techniques have been introduced in the literature; however, high PAPR reduction gain comes at the expense of computational complexity. In this paper, a novel selective mapping (SLM) scheme for PAPR reduction in OFDM-NOMA systems is proposed. By utilizing the structure of the OFDM-NOMA transmitter, the proposed SLM scheme achieves the same performance as that of the conventional SLM scheme while requiring less computational complexity.

Keywords: OFDM, NOMA, PAPR, SLM

1 Introduction

After the initial commercial 5G networks were deployed, academia and industry began to consider 6G mobile networks. Every decade, a new mobile generation is released. However, early work on 6G has begun in order to support new emerging applications that 5G networks are unable to support [1, 2]. Furthermore, the exponential growth in the number of smart devices and data traffic is expected to outstrip the capabilities of the 5G networks. According to the International Telecommunication Union, the global number of mobile broadband (MBB) subscribers will reach 17.1 billion by 2030. In addition, all subscribers have been estimated to consume approximately 250 GB of data per month by 2030, an increase from 5 GB in 2020. Furthermore, the global number of Internet of things devices is expected to increase to 97 billion by 2030, up from 7 billion in 2020 [1, 3]. As a result, 6G is expected to support new usage scenarios such as further-enhanced mobile broadband (FeMBB), ultra-massive machine-type communications

(umMTC), and extremely reliable and low-latency communications (ERLLC), as an improved version of the 5G usage scenarios, i.e., enhanced mobile broadband (eMBB), massive machine-type communications (mMTC), and reliable and low-latency communications (RLLC) [1, 2].

As a result, new enabling technologies are needed to support these new usage scenarios. As the backbone of cellular communication networks, multiple access techniques have played a critical role in the design of each generation of cellular networks. All successive generations of mobile networks (from 1 to 5G) have used orthogonal multiple access (OMA) techniques such as frequency division multiple access (FDMA), time division multiple access (TDMA), code division multiple access (CDMA), and orthogonal frequency division multiple access (OFDMA). Although OMA techniques prevent interference among users and require simple receivers, they waste spectrum resources by limiting the number of serviced users to the number of the orthogonal resource units (i.e., frequency, time, or code) at each cell. As a result, OMA cannot support massive connectivity which is critical in 6G. Non-orthogonal multiple access (NOMA) techniques, in contrast to conventional OMA, can increase spectrum efficiency and support massive connectivity by allowing an arbitrary number of users to share the same resource unit (i.e., time and frequency) at the same time. This qualifies NOMA for umMTC and ERLLC scenarios in 6G. NOMA outperforms OMA in terms of spectral efficiency (SE), user fairness, higher cell-edge throughput, and lower latency, according to several studies [4–6]. NOMA is clearly a promising candidate for 6G networks [7].

Many NOMA schemes have been proposed in the literature by industrial and academic communities. Generally, NOMA schemes are broadly classified into two types: power domain NOMA and code domain NOMA. The power domain NOMA (PD-NOMA) is simpler to implement than the code domain NOMA. As a result, PD-NOMA has generated increased interest in the literature [7]. Different users in PD-NOMA are assigned different power levels, based on their channel conditions. This paper is concerned with PD-NOMA.

The ability of orthogonal frequency division multiplexing (OFDM) to mitigate frequency selectivity, solve the delay spread problem in multipath channels, and reduce the complexity of the equalization process has drawn a lot of attention to a combination of NOMA and OFDM. Throughout this paper, OFDM-based PD-NOMA will be referred to as OFDM-NOMA. Given that OFDM was used in previous mobile generations (i.e., 4G and 5G), it is expected that OFDM-NOMA will be used in the upcoming 6G. However, the worst problem of OFDM-based systems, that is, a high peak-to-average power ratio (PAPR), will have an impact on OFDM-NOMA system performance. After passing through the nonlinear high power amplifier (HPA), the signal becomes distorted due to high PAPR. Unless the HPA works with a large input power back-off (IBO), this distortion results in bit error rate (BER) degradation and out-of-band (OOB) radiation. Large IBO, on the other hand, waste HPA efficiency. This means that the OFDM-NOMA system will exhibit some nonlinear distortion in order to preserve the HPA efficiency. As a result, in order to mitigate the effect of nonlinear distortion, the PAPR of the OFDM-NOMA system must be reduced [8].

Few studies have been conducted on the performance of OFDM-NOMA systems in the presence of nonlinear distortion. In [9], nonlinear distortion was modeled as a

residual hardware impairments (RHI) term, whereas in [10, 11], HPA was modeled as a polynomial. Both the polynomial model and the RHI term are insufficient to investigate the effect of the nonlinear HPA on the performance of the OFDM-NOMA system. In contrast, the authors of [8, 12, 13] used the Bussgang theorem to model HPA. This is a practical HPA model for investigating the impact of IBO on the performance of the OFDM-NOMA system. The Bussgang theorem was used to model HPA in this work.

There are also some works in the literature that aim to reduce the PAPR of the OFDM-NOMA signal. PAPR reduction using different precoding transform matrixes has piqued the interest of researchers due to its low computational complexity. In [14–18], authors reduced the PAPR of the OFDM-NOMA signal, or multicarrier-based NOMA, using discrete sine transform (DST), discrete cosine transform (DCT), Walsh–Hadamard transform (WHT), discrete Fourier transform (DFT), and hybrid Zadoff–Chu matrix transform (ZCT) with WHT, respectively. PAPR reduction using precoding transforms matrixes, on the other hand, has a small PAPR reduction gain. As a result, some researchers combined precoding techniques with the other PAPR reduction techniques to increase the PAPR reduction gain. For example, authors in [19] combined the DST precoding matrix and the dummy sequence insertion technique (DSI). Similarly, in [20], the discrete Hartley transform (DHT) precoding matrix was combined with the clipping technique. Similarly, the authors of [21] combined DCT with a filtering technique.

Furthermore, selective mapping (SLM) was used in [22, 23] to reduce the PAPR of multicarrier-based NOMA, due to the high PAPR reduction gain of the SLM technique. However, the conventional SLM technique necessitates a high value of computational complexity in exchange for a high PAPR reduction gain.

Previous studies that used SLM for PAPR reduction in NOMA-based systems [22, 23] did not care about SLM computational complexity. However, several studies have been proposed in the literature to reduce the computational complexity of SLM. Most of the existing works in the literature reduce the required number of inverse fast Fourier transform (IFFT) process by producing extra number of alternative signals through linear addition or cyclic shifting of conventionally generated alternative signals in the time domain.

In [24], a linear addition-based method called Green-OFDM was proposed to reduce the SLM computational complexity; however, this method requires the phase rotation vectors involved in the linear addition process to be orthogonal. To increase the number of alternatives to more than twice the square of the number of IFFT processes employed, an enhanced version of the Green-OFDM method [24] was developed in [25]. The scheme of [25] reduces the computational complexity by fifty percent. In [26], a different linear addition-based method was utilized to lower SLM computational complexity by roughly seventy percent. This method is not reliant on orthogonal phase rotation vectors. Similar to this, the authors of [27] developed a linear addition-based method that makes use of the real and imaginary halves of alternative signals that are conventionally generated. However, when the number of alternative signals raises, linear addition-based methods experience a strong correlation among the alternative signals, which degrades their ability to reduce PAPR compared to the conventional SLM technique [28]. In addition, linear addition-based methods degrade the BER performance compared to the

conventional SLM technique due to the probable attenuation of the power of some subcarriers as a result of the linear addition process [29].

The authors in [30, 31] combine linear addition with cyclic shifting to increase the number of possible alternative signals. However, the alternative signals created by cyclic shifting based or linear addition-based methods suffer from considerable correlation.

To generate many uncorrelated alternative signals, authors in [32, 33] used a low-complexity SLM technique based on a conversion matrix. The conversion matrix is generated by a circular shift of a periodic phase vector. Comparing the conversion matrix based method to the conventional SLM technique, the PAPR reduction performance is slightly worse, but the computational complexity is reduced. However, this method cannot generate many alternative signals [28]. To reduce computational complexity more, the authors of [28] combined a linear addition-based method with the conversion matrix based method; nevertheless, the results in [28] revealed that the PAPR reduction performance was worse than that of the conversion matrix based method.

Recently, many metaheuristic algorithms are used to reduce the SLM technique's computational complexity, including the artificial bee colony algorithm [34], the quantum inspired evolutionary algorithm [35], the migrating birds' optimization algorithm [36], and the firefly algorithm [37]. However, metaheuristic algorithms degrade the PAPR reduction performance, unless use the same number of IFFT processes as the conventional SLM. In this case, metaheuristic algorithms increase the computational complexity and improve the PAPR reduction gain more than the conventional SLM technique. This is because the original purpose of metaheuristic algorithms was to find a suboptimal solution when the ideal solution cannot be found by exhaustive search.

Motivated by the limitations of previous works, this article proposes a novel low-complexity SLM scheme that achieves PAPR reduction gain the same as the conventional SLM technique without degrading the BER performance. The structure of the OFDM-NOMA transmitter will be used in this article to reduce the computational complexity of SLM. This article's contribution can be summarized as follows:

- This paper proposes a novel SLM technique for reducing PAPR in OFDM-NOMA systems. The proposed technique achieves the same performance as the conventional SLM technique while requiring significantly less computational complexity. Furthermore, increasing the PAPR reduction gain increases computational complexity reduction in the proposed SLM technique.
- Unlike previous works, this one investigates the impact of the proposed PAPR reduction technique on the sum rate capacity of the OFDM-NOMA system. In addition, the effect of the proposed PAPR reduction technique on the asymptotic upper limit of the sum rate capacity in the presence of nonlinear distortion in the OFDM-NOMA system has been investigated.
- The effect of PAPR reduction on BER performance in the OFDM-NOMA system in the presence of nonlinear distortion was investigated in this work for different modulation orders.

The remaining sections of this article are organized as follows: Section 2 describes the OFDM-NOMA system model. Section 3 investigates the effect of nonlinear distortion

on the OFDM-NOMA system. The conventional SLM in the OFDM-NOMA system is described Section 4. Section 5 introduces the proposed SLM technique. Simulation and results are discussed in Section 6. Finally, the conclusion is provided in Section 7.

2 OFDM-NOMA system

Consider a downlink (DL) OFDM-NOMA system in which the transmitter at the BS superimposes data from M users on the same subcarrier, as opposed to an OFDM-OMA system in which data from a single user is transmitted on each subcarrier. The complex baseband representation of the BS's transmitted OFDM-NOMA signal is given by:

$$x_n = \frac{1}{\sqrt{N}} \sum_{k=1}^{K} \left(\sum_{m=1}^{M} \sqrt{\alpha_{k,m} P_k} A_{k,m} \right) e^{-j\frac{2\pi nk}{N}} \quad 0 \le n \le N-1 \,, \tag{1}$$

where K represents the number of subcarriers in the OFDM symbol, M represents the number of superposed users on each subcarrier, N represents the number of time domain samples of the OFDM symbol, $A_{k,m}$ represents the mth user's data on the kth subcarrier, P_k represents the assigned power to the kth subcarrier, and $\alpha_{k,m}$ represents the power allocation ratio of the mth user's on the kth subcarrier. Practically, not all subcarriers are bearing data, few subcarriers on the edges of the OFDM-NOMA symbol are set to zero to avoid interference among successive symbols. Let K_D represent the number of data subcarriers, the remaining $(K - K_D)$ subcarriers are null and serving as a guard band on the edges, i.e., $(K - K_D)/2$ subcarrier per side. The input vector to the IFFT can be written mathematically as; $\boldsymbol{A} = \left[0, .., 0, \; A_0 \; \cdots \; A_k \; \cdots \; A_{(K_D-1)}, \; 0, .., 0 \right]_{1\times \mathrm{K}}$, where$A_k = \sum_{m=1}^{M} A_{k,m}$. Equation (1) shows that the number of time domain samples of the OFDM-NOMA symbol is equal to the number of subcarriers, i.e.,$N = K$, when the Nyquist rate is the sampling frequency. On the other hand, in the case of L times oversampled signal, the number of time domain samples in the OFDM-NOMA symbol is L times the symbol's subcarriers number. The oversampled signal is obtained by inserting $(L-1)K$ zeros in the middle of the input vector$\boldsymbol{A}$, in the frequency domain, before IFFT process.

The power allocation ratio $\alpha_{k,m}$ in (1) is inversely proportional to the user's channel condition. If the users are in a descending order by their channel condition, with the first user being the near user (NU) and the latest user (i.e., Mth user) being the far user (FU), then $\alpha_{k,1} < \cdots < \alpha_{k,m} < \cdots < \alpha_{k,M}$, under the condition $\sum_{m=1}^{M} \alpha_{k,m} = 1$[38]. A block diagram representation of the DL OFDM-NOMA system is depicted in Fig. 1.

At the mth user's terminal, the received signal on the kth subcarrier is given by:

$$Y_{k,m} = H_{k,m} \left(\sum_{m=1}^{M} \sqrt{\alpha_{k,m} P_k} A_{k,m} \right) + N_{k,m} \quad \begin{matrix} 1 \le k \le K \\ 1 \le m \le M \end{matrix} , \tag{2}$$

where $N_{k,m}$ represents the additive white Gaussian noise (AWGN) at the mth user's terminal on subcarrier k in the frequency domain with zero mean and $\sigma_{k,m}^2$ variance and $H_{k,m}$ represents the channel frequency response, between the BS and the mth user's terminal, of the channel $h_{k,m} = g_{k,m}/\sqrt{1 + d_m^{\propto}}$ where d_m represents the distance between the BS and the mth user's terminal, $\propto$ represents the path loss exponent, and $g_{k,m}$ represents the small scale fading coefficient between the BS and the mth user's terminal on the kth subcarrier [39]. Successive interference cancellation (SIC) is used in the receiver

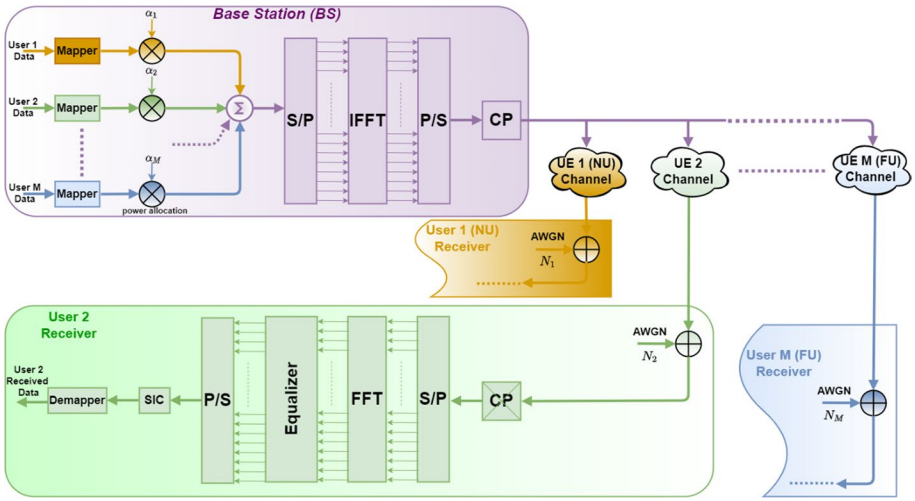

Fig. 1 Block diagram of DL OFDM-NOMA system

to separate out each user's signal and get rid of interference from the other superposed users. By subtracting decoded signals of weaker users (i.e., user $i\text{th}|_{i>m}$) from the received signal at the mth user terminal. The signals of the stronger users (i.e., user $i\text{th}|_{i<m}$) are left as interference. Thus, the normalized achievable data rate of the mth user is given as:

$$R_m = \sum_{k=1}^{K} \log_2\left(1+\gamma_{k,m}\right), \tag{3}$$

where

$$\gamma_{k,m} = \frac{P_k\left|H_{k,m}\right|^2\alpha_{k,m}}{\left(P_k\left|H_{k,m}\right|^2\sum_{i=1}^{m-1}\alpha_{k,i}\right)+\sigma_{k,m}^2} = \frac{\rho_{k,m}\left|H_{k,m}\right|^2\alpha_{k,m}}{\left(\rho_{k,m}\left|H_{k,m}\right|^2\sum_{i=1}^{m-1}\alpha_{k,i}\right)+1}, \tag{4}$$

where $\gamma_{k,m}$ and $\rho_{k,m} \triangleq P_k/\sigma_{k,m}^2$ are the signal-to-interference-plus-noise ratio (SINR) and the signal-to-noise ratio (SNR) of the mth user over the kth subcarrier, respectively. The first term in the denominator of (4) becomes 0 in $\gamma_{k,1}$, i.e., at NU [8]. Finally, the total sum rate capacity is computed as shown below [8];

$$R_{\text{Total}} = \sum_{m=1}^{M} R_m = \sum_{m=1}^{M}\log_2\prod_{k=1}^{K}\left(1+\frac{\rho_{k,m}\left|H_{k,m}\right|^2\alpha_{k,m}}{\left(\rho_{k,m}\left|H_{k,m}\right|^2\sum_{i=1}^{m-1}\alpha_{k,i}\right)+1}\right), \tag{5}$$

3 PAPR problem and nonlinearity in OFDM-NOMA system

The characteristics of OFDM-NOMA signal are the same as those of the conventional OFDM-OMA signal; the real (a_n) and imaginary (b_n) parts of the OFDM-NOMA symbol ($x_n = a_n + jb_n$) follow the Gaussian distribution due to the summation of a large number of weighted sinusoidal signals as per central limits theorem. As a result, the absolute value ($|x_n|$) and the power ($|x_n|^2$) of the OFDM-NOMA symbol

are distributed according to Rayleigh and chi-squared distributions, respectively. The maximum value of the OFDM-NOMA symbol power is very large compared to the average value of the OFDM-NOMA symbol power, indicating that the PAPR of the OFDM-NOMA symbol is indeed very large, according to the chi-squared distributions. The PAPR of the OFDM-NOMA symbol is written mathematically as:

$$\xi = \frac{\underset{0\le n\le N-1}{\boldsymbol{max}}\left[|x_n|^2\right]}{\boldsymbol{E}\left[|x_n|^2\right]}, \tag{6}$$

where $\boldsymbol{max}[]$ and $\boldsymbol{E}[]$ are the maximum and average OFDM-NOMA symbol power values [40]. Because the PAPR is a random variable, the complementary cumulative distribution function (CCDF) is commonly used to describe it. CCDF expresses the likelihood that the OFDM-NOMA symbol's PAPR is greater than or equal to a given threshold (ξ_{th}). The oversampled OFDM-NOMA signals' CCDF is given by:

$$pr(\xi \ge \xi_{th}) = 1 - \exp\left(-Ke^{-\xi_{th}}\sqrt{\frac{\pi}{3}\log K}\right), \tag{7}$$

where oversampling by four times larger than the Nyquist rate (i.e., $L=4$) is sufficient to simulate the continuous time OFDM-NOMA signal and $pr()$ represents the probability [41].

When the transmitted OFDM-NOMA signal passes through the nonlinear HPA, it will be subjected to nonlinear distortion unless the HPA works with IBO equal to the transmitted OFDM-NOMA signal's PAPR. However, this is an impractical solution and the transmitted OFDM-NOMA signal will suffer from nonlinear distortion when it passes through the nonlinear HPA, depending on the value of the IBO. Figure 2 shows the effect of IBO on the integrity of the transmitted signal and the efficiency of the HPA. It is obvious that the HPA efficiency reaches its maximum value at the saturation level; as a result, the HPA efficiency is inversely proportional to the IBO. For instance, a small IBO results in high-efficiency HPA but exposes the OFDM signal (red dotted line) to nonlinear distortion. On the other hand, increasing the IBO value reduces HPA efficiency while protecting the OFDM signal (green solid line) from nonlinear distortion. IBO is mathematically represented as [40]:

$$\text{IBO} = \frac{x_{\text{sat}}^2}{E\left[|x_n|^2\right]}, \tag{8}$$

where x_{sat} represents the saturation level of the linearized HPA, also called soft limiter (SL). In the presence of nonlinear distortion, the received OFDM-NOMA signal is not the same as in (2); instead, it is modified according to Bussgang theorem as follows [8]:

$$Y_{k,m} = H_{k,m}\left(\mathcal{T}\sum_{m=1}^{M}\sqrt{\alpha_{k,m}P_k}A_{k,m} + D_k\right) + N_{k,m} \quad \begin{matrix} 1 \le k \le K \\ 1 \le m \le M \end{matrix}, \tag{9}$$

where D_k represents the nonlinear distortion noise on the k_{th} subcarrier in the frequency domain and $\mathcal{T}$ represents the attenuation factor due to nonlinear distortion, which is given by [42]:

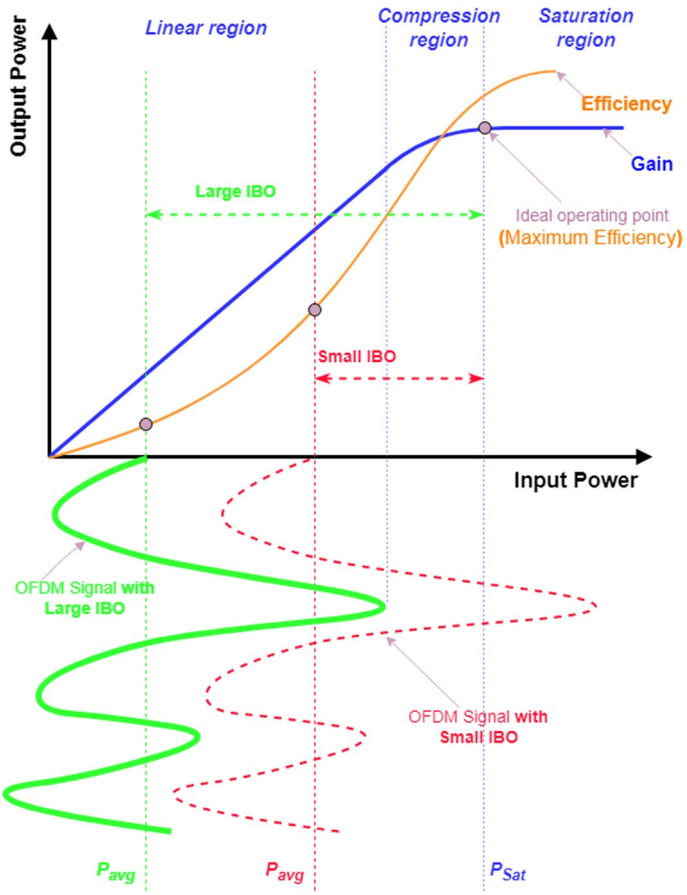

Fig. 2 Effect of IBO on the integrity of the transmitted signal and the efficiency of the HPA [41]

$$\mathcal{T} = 1 - e^{-\mathcal{B}^2} + \frac{\sqrt{\pi}\mathcal{B}}{2} erfc(\mathcal{B}), \tag{10}$$

where $erfc()$ represents the complementary error function and $\mathcal{B}$ denotes the clipping ratio which is given by the square root of the IBO as follows [42]:

$$\mathcal{B} = \frac{x_{sat}}{\sqrt{\boldsymbol{E}\left[|x_n|^2\right]}}, \tag{11}$$

The OFDM-NOMA signal received on the k_{th} subcarrier (9) can be rewritten as follows [8]:

$$\begin{aligned} Y_{k,m} = & \underbrace{\mathcal{T}\sqrt{P_k}H_{k,m}\sqrt{\alpha_{k,m}}A_{k,m}}_{\text{Desired Signal}} + \underbrace{\mathcal{T}\sqrt{P_k}H_{k,m}\sum_{i=m+1}^{M}\sqrt{\alpha_{k,i}}A_{k,i}}_{\text{SIC removed}} \\ & + \underbrace{\mathcal{T}\sqrt{P_k}H_{k,m}\sum_{i=1}^{m-1}\sqrt{\alpha_{k,i}}A_{k,i}}_{\text{IUI}} + \underbrace{H_{k,m}D_k}_{\text{Distortion}} + \underbrace{N_{k,m}}_{\text{Noise}} \end{aligned} \tag{12}$$

The desired signal is represented by the first term in (12), while the second and third terms represent the interference from the weaker and the stronger users on the mth user, respectively. The SIC will remove the second term, but the inter-user interference (IUI) in the third term will not be removed. Nonlinear distortion on the kth subcarrier is represented in the fourth term, while the last term in (12) represents the AWGN on the kth subcarrier at the mth user terminal.

The signal to interference, noise, and distortion ratio (SINDR) on the kth subcarrier at the mth user terminal is then calculated as follows:

$$\gamma_{k,m} = \frac{\mathcal{T}^2 P_k \left|H_{k,m}\right|^2 \alpha_{k,m}}{\left(\mathcal{T}^2 P_k \left|H_{k,m}\right|^2 \sum_{i=1}^{m-1} \alpha_{k,i}\right) + \left(1 - e^{-\mathcal{B}^2} - \mathcal{T}^2\right) P_k \left|H_{k,m}\right|^2 + \sigma_{k,m}^2}, \tag{13}$$

where $\left(1 - e^{-\mathcal{B}^2} - \mathcal{T}^2\right) P_k$ represents the variance of the nonlinear distortion noise, and the first term in the denominator of (13) will be 0 at $\gamma_{k,1}$, i.e., at the NU receiver. As a result, by substituting Eq. (13) into Eq. (3), the sum rate capacity of all users across all subcarriers is given by:

$$R_{\text{Total}} = \sum_{m=1}^{M} \log_2 \prod_{k=1}^{K} \left(1 + \frac{\mathcal{T}^2 \rho_{k,m} \left|H_{k,m}\right|^2 \alpha_{k,m}}{\left(\mathcal{T}^2 \rho_{k,m} \left|H_{k,m}\right|^2 \sum_{i=1}^{m-1} \alpha_{k,i}\right) + \rho_{k,m} \left|H_{k,m}\right|^2 \left(1 - e^{-\mathcal{B}^2} - \mathcal{T}^2\right) + 1}\right), \tag{14}$$

Finally, the asymptotic upper limit of the sum rate capacity, when SNR is very high (i.e.,$\rho_{k,m} \to \infty$), is given by [8]:

$$\begin{aligned} R_{\text{Total}}^{\infty} &= \sum_{m=1}^{M} \log_2 \prod_{k=1}^{K} \left(1 + \frac{\mathcal{T}^2 \alpha_{k,m}}{\left(\mathcal{T}^2 \sum_{i=1}^{m-1} \alpha_{k,i}\right) + \left(1 - e^{-\mathcal{B}^2} - \mathcal{T}^2\right)}\right) \\ &\approx \sum_{m=1}^{M} \log_2 \prod_{k=1}^{K} \left(1 + \frac{\alpha_{k,m}}{\sum_{i=1}^{m-1} \alpha_{k,i} + \frac{1}{e^{\mathcal{B}^2} - 1}}\right), \end{aligned} \tag{15}$$

where $\mathcal{T} \approx 1 - e^{-\mathcal{B}^2}$ at large $\mathcal{B}$. This asymptotic upper limit of the sum rate capacity is determined by the IBO. Again, the first term in the denominator of (14) and (15) is zero at $m = 1$. So, to increase $R_{\text{Total}}^{\infty}$, IBO must be increased, or the PAPR value of the OFDM-NOMA signal must be decreased. Many PAPR reduction techniques have been introduced in the literature, with SLM being one of the most powerful. However, the SLM technique's high PAPR reduction comes at the expense of computational complexity. The conventional SLM technique and the proposed SLM technique for OFDM-NOMA will be described in the following two sections, respectively.

4 Conventional SLM technique

In conventional SLM U alternatives for the OFDM-NOMA symbol are generated in the frequency domain before being converted into the time domain by the IFFTs. In the time domain, the u_{th} alternative with the lowest PAPR is chosen and transmitted, as illustrated in Fig. 3. To generate U alternatives for the OFDM-NOMA symbol $\boldsymbol{x} = \begin{bmatrix} x_0 & x_1 & \cdots & x_n & \cdots & x_{N-1} \end{bmatrix}$, the input data block

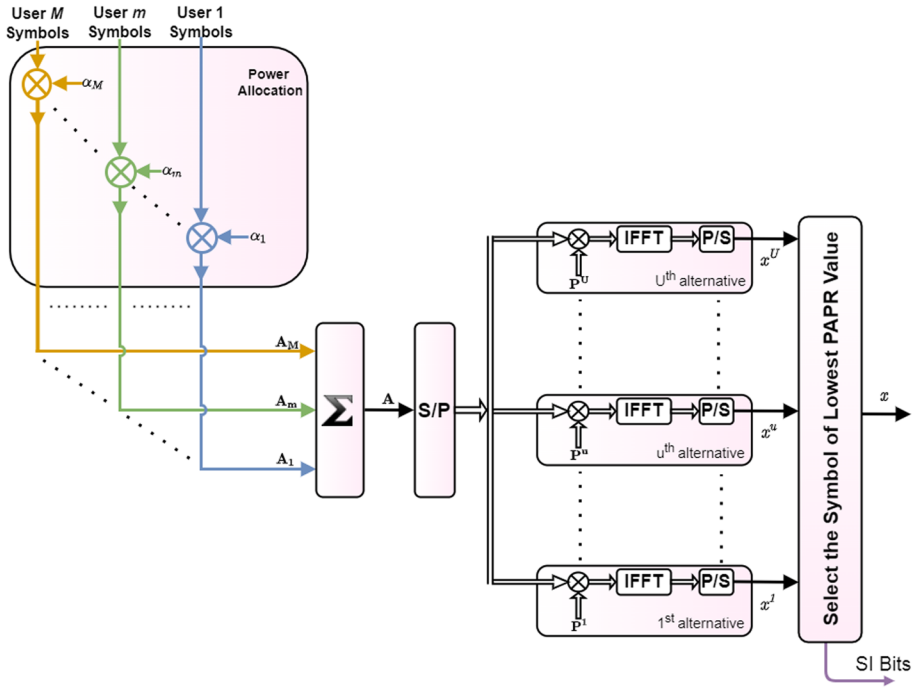

Fig. 3 Block diagram of the conventional SLM technique for DL OFDM-NOMA system

$\boldsymbol{A} = \left[\, A_0 \; A_1 \;\; \cdots \; A_k \;\; \cdots \; A_{K-1} \,\right]$ is multiplied by a predefined set (i.e., known at both BS and UEs) of phase rotation vectors $\boldsymbol{P}^u = \left[\, p_0^u \; p_1^u \;\; \cdots \; p_k^u \;\; \cdots \; p_{K-1}^u \,\right]$ in the frequency domain, where $1 \leq u \leq U$, $p_k^u = e^{j\theta_k^u}$ and $\theta_k^u \epsilon [0,\, 2\pi)$. Following that, in the time domain, U alternatives of the OFDM-NOMA symbol $\boldsymbol{x}$ are generated, such that $\boldsymbol{x}^u = \boldsymbol{IFFT}(\boldsymbol{A} \cdot \boldsymbol{P}^u)$, where $(\cdot)$ denotes elementwise multiplication. Finally, $\boldsymbol{x}^{\widehat{u}}$ with the lowest PAPR among the U alternatives is chosen, as follows [43]:

$$\widehat{u} = \underset{1 \leq u \leq U}{\textbf{argmin}} \left(\frac{\underset{0 \leq n \leq N-1}{\boldsymbol{max}} \left| x_n^u \right|^2}{\boldsymbol{E}\left[\left| x_n^u \right|^2 \right]} \right), \tag{16}$$

The PAPR reduction performance of SLM is obviously dependent on the number of alternatives U and the phase rotation vectors $\boldsymbol{P}^u$ design. In general, phase rotation elements p_k^u are complex numbers with unity amplitude and chosen at random from the following sets $p_k^u \in \{\pm 1\}$ or $p_k^u \in \{\pm 1, \pm j\}$ to reduce the computational complexity, so no actual multiplications will be required in $(\boldsymbol{A} \cdot \boldsymbol{P}^u)$. The CCDF of the reduced PAPR after SLM is then given by [44]:

$$\boldsymbol{pr}\{\gamma \geq \gamma_{th}\} = \left[1 - exp\left(-Ne^{-\gamma_{th}} \sqrt{\frac{\pi}{3} \boldsymbol{log} N} \right) \right]^U, \tag{17}$$

As a result, PAPR reduction gain for a certain clipping probability p due to the SLM technique is given as [45]:

$$G = -10\boldsymbol{log}\left(\frac{\gamma_{th}^{\mathrm{SLM}}}{\gamma_{th}}\right) = -10\boldsymbol{log}\left(\boldsymbol{ln}\left(\frac{\boldsymbol{ln}\left(1-p^{1/U}\right)}{N\sqrt{\frac{\pi}{3}\boldsymbol{log}N}}\right)/\boldsymbol{ln}\left(\frac{\boldsymbol{ln}(1-p)}{N\sqrt{\frac{\pi}{3}\boldsymbol{log}N}}\right)\right), \quad (18)$$

This means that for the same IBO value (i.e., same clipping probability p) SLM equivalently reduces HPA clipping severity $\mathcal{B}$ by the amount G (i.e.,$\mathcal{B}^{\mathrm{SLM}} = \mathcal{B} + G$). This G gain in PAPR reduction comes at the expense of computational complexity and side information bits.

The computational complexity of SLM is composed of U of IFFT blocks and U of PAPR calculation (metric) processes. It is known that the computational complexity of N-point IFFT consists of $\left(2N\mathbf{log}_2 N\right)$ real multiplications and $\left(3N\mathbf{log}_2 N\right)$ real additions. However, because SLM does not change the signal average power, the PAPR calculation process is shortened to an absolute value squaring process. As a result, the computational effort of the PAPR calculation process consists of $(2N)$ real multiplications and (N) real additions. As a result, the computational complexity of SLM is given by [46]:

$$\mathcal{A}_{\mathrm{SLM-conv}} = 3UN\boldsymbol{log}_2 N + UN, \quad (19a)$$

$$\mathcal{M}_{\mathrm{SLM-conv}} = 2UN\mathbf{log}_2 N + 2UN, \quad (19b)$$

where $\mathcal{A}$ and $\mathcal{M}$ represent the number of real additions and multiplications, respectively. This means that the computational complexity of SLM is proportional to the required PAPR reduction gain and is dependent on the number of alternatives. As a result, increasing the PAPR reduction gain comes at the expense of increased computational complexity.

Similarly, increasing the number of alternatives will increase the required number of side information (SI) bits $\lceil \mathbf{log}_2 U \rceil$ [46]. Assume a channel coding technique with code rate R_c is used to protect the SI bits and binary phase shift keying (BPSK) is used to modulate the SI bits. Then, the number of the available subcarriers will be reduced to $\left(K - \left(\lceil \mathbf{log}_2 U \rceil / R_c\right)\right)$, which, in turn, reduces the spectrum efficiency by $\left(1 - \left(\lceil \mathbf{log}_2 U \rceil / NR_c\right)\right)$.

5 Proposed SLM technique

As demonstrated in the preceding section, the conventional SLM technique's high PAPR reduction gain comes at the expense of computational complexity and spectral efficiency. In this section, a novel SLM scheme is proposed to reduce computational complexity and the number of SI bits required by utilizing the structure of the NOMA technique.

The proposed SLM does not generate the U alternatives of the OFDM-NOMA symbol after power allocation and superpositioning. Instead, before superpositioning, U alternatives are generated for each user symbol. In the frequency domain after power allocation, the data block of each user $\boldsymbol{A}_m = \left[\, A_{0,m}\ A_{1,m}\ \cdots\ A_{k,m}\ \cdots\ A_{K-1,m} \,\right]$ is multiplied by a predefined set of phase rotation vectors $\boldsymbol{p}_m^u = \left[\, p_{0,m}^u\ p_{1,m}^u\ \cdots\ p_{k,m}^u\ \cdots\ p_{K-1,m}^u \,\right]$, where $1 \le m \le M$ and $1 \le u \le U$. Then, U alternatives of each user are transformed into the time domain before superpositioning, such that $\boldsymbol{x}_m^u = \boldsymbol{IFFT}\left(\boldsymbol{A}_m \bullet \boldsymbol{p}_m^u\right)$. As a result, as shown in Fig. 4, there will be $I = U^M$ possible superpositioning vectors generated by UM IFFT blocks. Finally, the OFDM-NOMA symbol with the lowest PAPR

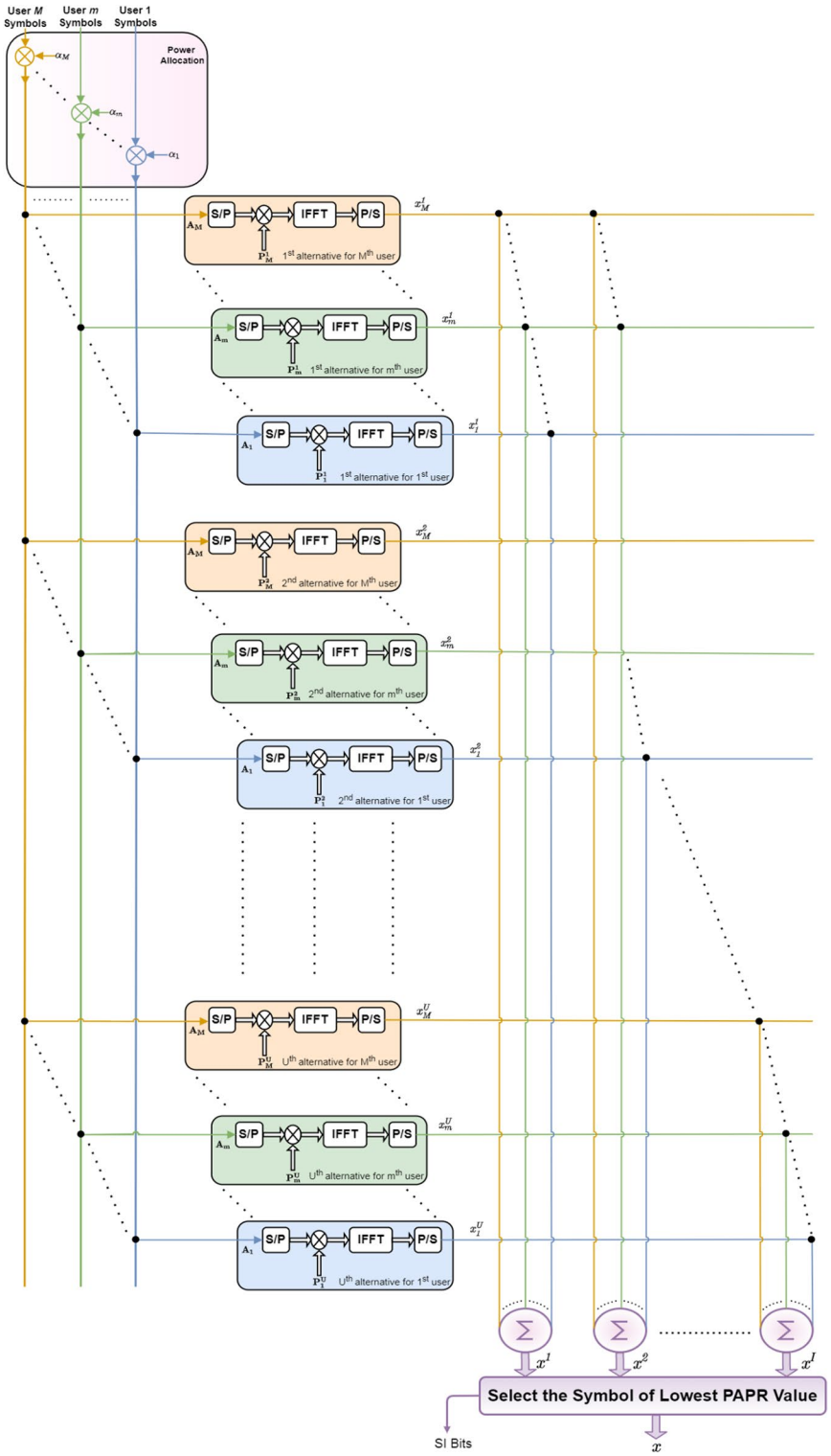

Fig. 4 Block diagram of the proposed SLM technique for DL OFDM-NOMA system

value among the $I = U^M$ alternatives is chosen and transmitted such as $\boldsymbol{x} = \sum_{m=1}^{M} \boldsymbol{x}_m^{\widehat{u}_m}$ where $\widehat{u}_m \in [1, U]$ is the index of the optimum phase rotation vector for user m defined as follows:

$$\left[\begin{array}{cccc} \widehat{u}_1 & \cdots & \widehat{u}_m & \cdots \ \widehat{u}_M \end{array}\right] = \underset{\left[\begin{array}{ccc} u_1 & \ldots & u_M \end{array}\right]}{\textbf{argmin}} \left(\frac{\underset{0 \le n \le N-1}{\boldsymbol{max}} \left| \sum_{m=1}^{M} x_{n,m}^{u} \right|^2}{\boldsymbol{E}\left[\left| \sum_{m=1}^{M} x_{n,m}^{u} \right|^2 \right]} \right), \tag{20}$$

It is obvious that the proposed SLM technique requires fewer IFFT processes than the conventional SLM technique to generate the same number of alternative signals. Explicitly, to generate $I = U^M$ alternative signals, conventional SLM technique must perform $\left(U^M\right)$ IFFT process, while the proposed SLM technique reduces the required number of IFFT processes to (UM). This is because the proposed SLM technique carries out the superposition of users' signals in the time domain, while the system-based conventional SLM technique carries out the superposition of users' data in the frequency domain. Due to superpositioning in the time domain, there are U^M of possible permutations for combining the signals of the M users, given that there are U alternatives for each one of the M users. For example, if an OFDM-NOMA system with $M = 2$ wants to generate $I = 16$ $(= U^M = 4^2)$ alternative signals, the proposed SLM technique can do that using 8 $(= U \times M = 4 \times 2)$ IFFT processes. On the other hand, conventional SLM technique needs 16 IFFT process to produce the $I = 16$ alternative signals. The previous example can be further illustrated as follows; Let $\boldsymbol{x}_1^1, \boldsymbol{x}_1^2, \boldsymbol{x}_1^3$, and $\boldsymbol{x}_1^4$ be the four alternatives of the 1'st user signal, generated by four IFFT processes, and $\boldsymbol{x}_2^1, \boldsymbol{x}_2^2, \boldsymbol{x}_2^3$, and $\boldsymbol{x}_2^4$ be the four alternatives of the 2'nd user signal. This results in 16 $(= U^M = 4^2)$ possible permutation for superpositioning of time domain signals of user 1 and user 2, given as follows; $\left(\boldsymbol{x}_1^1 + \boldsymbol{x}_2^1\right), \left(\boldsymbol{x}_1^1 + \boldsymbol{x}_2^2\right), \left(\boldsymbol{x}_1^1 + \boldsymbol{x}_2^3\right), \left(\boldsymbol{x}_1^1 + \boldsymbol{x}_2^4\right), \left(\boldsymbol{x}_1^2 + \boldsymbol{x}_2^1\right), \left(\boldsymbol{x}_1^2 + \boldsymbol{x}_2^2\right), \left(\boldsymbol{x}_1^2 + \boldsymbol{x}_2^3\right), \left(\boldsymbol{x}_1^2 + \boldsymbol{x}_2^4\right)$, $\left(\boldsymbol{x}_1^3 + \boldsymbol{x}_2^1\right), \left(\boldsymbol{x}_1^3 + \boldsymbol{x}_2^2\right), \left(\boldsymbol{x}_1^3 + \boldsymbol{x}_2^3\right), \left(\boldsymbol{x}_1^3 + \boldsymbol{x}_2^4\right), \left(\boldsymbol{x}_1^4 + \boldsymbol{x}_2^1\right), \left(\boldsymbol{x}_1^4 + \boldsymbol{x}_2^2\right), \left(\boldsymbol{x}_1^4 + \boldsymbol{x}_2^3\right)$, and $\left(\boldsymbol{x}_1^4 + \boldsymbol{x}_2^4\right)$.

Then, the one with the lowest PAPR value among the 16 alternatives of the OFDM-NOMA signal is selected and transmitted.

On the receiver side, each user must be aware of the selected phase vector $\widehat{\mathrm{u}} = \left[\begin{array}{cccc} \widehat{\mathrm{u}}_1 & \cdots & \widehat{\mathrm{u}}_\mathrm{m} & \cdots \ \widehat{\mathrm{u}}_\mathrm{M} \end{array}\right]$ to correctly decode its data. As a result, the number of the required SI bits per user is $\lceil \mathbf{log}_2 U \rceil$ and the total number of the required SI bits for all users is $M\lceil \mathbf{log}_2 U \rceil$, assuming all users have the same number of alternatives, i.e., U. Furthermore, the total number of the required SI bits of the proposed SLM scheme may be reduced from $M\lceil \mathbf{log}_2 U \rceil$ to $\lceil \mathbf{log}_2 U \rceil$ if NOMA is used in their transmission rather than OMA, i.e., SI bits of all users can be superpositioned with different power levels. This, however, may increase the BER.

For the same number of alternatives U^M, the proposed SLM scheme requires computational complexity less than that required by the conventional SLM scheme. The computational complexity of the proposed SLM technique is composed of UM of IFFT process, U^M of PAPR calculation, and U^M of superposition process. The computational complexity of PAPR calculation and the N-point IFFT process are described in the previous section. The computational complexity of the superposition process

consists of $(M-1)$ of $2N$ real addition, i.e., $2N(M-1)$ real addition. As a result, the proposed SLM scheme's computational complexity is given by:

$$\mathcal{A}_{\text{SLM-prop}} = 3UMN\boldsymbol{log}_2 N + U^M N + 2U^M N(M-1), \tag{21a}$$

$$\mathcal{M}_{\text{SLM-prop}} = 2UMN\mathbf{log}_2 N + 2U^M N, \tag{21b}$$

where $\mathcal{A}$ and $\mathcal{M}$ represent the number of real additions and multiplications, respectively. The third term in Eq. (21a) is caused by user superposition.

The computational complexity reduction ratio (CCRR) is computed as $\left(1 - \frac{CC \text{ of proposed SLM}}{CC \text{ of conventional SLM}}\right) \times 100\%$ [47]. As a result, the CCRR of the proposed SLM in terms of $\mathcal{A}$ and $\mathcal{M}$ for the same number of alternatives (I) as the conventional SLM is given, respectively, by:

$$\text{CCRR}^{\mathcal{A}} = \frac{3\boldsymbol{log}_2 N}{1+3\boldsymbol{log}_2 N} \times \frac{I - \lceil \sqrt[M]{I} \rceil M - \frac{2I}{3\boldsymbol{log}_2 N}(M-1)}{I} \times 100\%, \tag{22a}$$

$$\text{CCRR}^{\mathcal{M}} = \frac{\boldsymbol{log}_2 N}{1+\boldsymbol{log}_2 N} \times \frac{I - \lceil \sqrt[M]{I} \rceil M}{I} \times 100\%, \tag{22b}$$

where $I = U$ in the case of conventional SLM and $I = U^M$ in the case of proposed SLM.

6 Results and discussion

The proposed SLM technique's performance will be compared to that of the conventional SLM technique in terms of PAPR reduction gain, sum rate capacity, computational complexity, and users' BER in this section. The simulation parameters are listed in Table 1.

Figure 5 compares the PAPR reduction gain of the proposed and conventional SLM techniques for different number of alternatives, i.e., $I = 64$ and 256. It should be noted

Table 1 Simulation parameters

Simulation parameter	Value		
Number of OFDM symbols	10^5		
Number of subcarriers (K)	256		
Number of data subcarriers (K_D)	200		
Channel	Multipath (Rayleigh channel)		
Channel estimation	Ideal		
Path loss exponent (α)	2.8		
Number of users (M)	2		
Space between users (meters)	50		
Power allocation ratios (α_{FU}/α_{NU})	(0.8/.2)		
HPA model	Soft limiter (SL)		
Oversampling factor (L)	4		
Number of alternatives (I)	16, 64, and 256		
Modulation type and order (FU/NU)	(4-QAM/4-QAM)	(4-QAM/16-QAM)	(4-QAM/64-QAM)
IBO (dB)	2	4	5

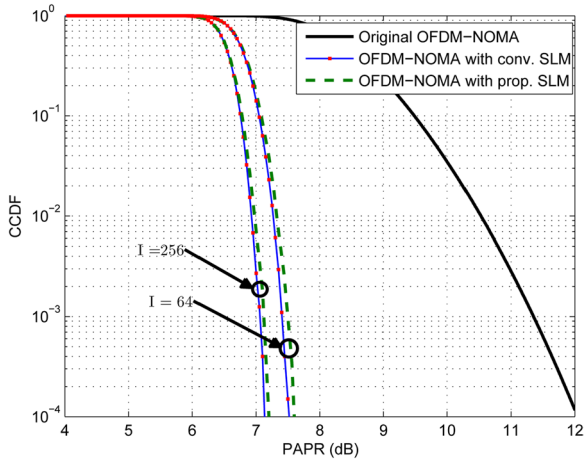

Fig. 5 PAPR reduction performance of conventional and proposed SLM techniques with different number of alternatives, i.e.,$I = 64, 256$

that the PAPR reduction performance of both conventional and proposed SLM techniques is the same.

Furthermore, Fig. 6 compares the sum rate capacity of OFDM-NOMA in the presence of the nonlinear distortion with and without the use of SLM techniques, as well as the sum rate capacity of the ideal OFDM-NOMA and the ideal OFDM-OMA, i.e., without the nonlinear distortion. It is obvious that both SLM techniques, conventional and proposed, improve sum rate capacity in the presence of nonlinear distortion. It is also worth noting that increasing the number of SLM alternatives raises the saturation level in the presence of nonlinear distortion. Surprisingly, the sum rate capacity of the proposed SLM technique is slightly higher than that of the conventional SLM technique, as the former requires fewer SI bits than the latter.

As previously stated, nonlinear distortion not only reduces the sum rate capacity but also causes it to be saturated to an upper limit that depends only on the IBO as shown in (15). The effect of using the SLM technique to improve the asymptotic upper limit of the sum rate capacity in the presence of the nonlinear distortion is investigated in Fig. 7, as per (15). Figure 7 compares the asymptotic upper limit of the sum rate capacity versus IBO before and after using the SLM technique with various numbers of alternatives (i.e., $I = 16, 64, 256$). In the presence of nonlinear distortion, it is obvious that increasing the number of alternatives raises the upper limit of the sum rate capacity. Furthermore, the proposed SLM technique is a bit better than the conventional SLM technique due to a reduction in the required SI bits in the proposed SLM technique over the conventional SLM technique. Notably, the SLM technique has no effect on the asymptotic upper limit of the sum rate capacity at low IBO.

Figure 8a and b compares the computational complexity of the proposed SLM technique and the conventional SLM technique in terms of the number of RA ($\mathcal{A}_{\text{SLM}}$) and number of RM ($\mathcal{M}_{\text{SLM}}$), respectively. The proposed SLM technique has the same performance as the conventional SLM technique while requiring significantly less computational complexity. Furthermore, increasing the number of users reduces the computational complexity required in the proposed SLM technique. It is clear that the computational complexity of the proposed SLM technique decreases by

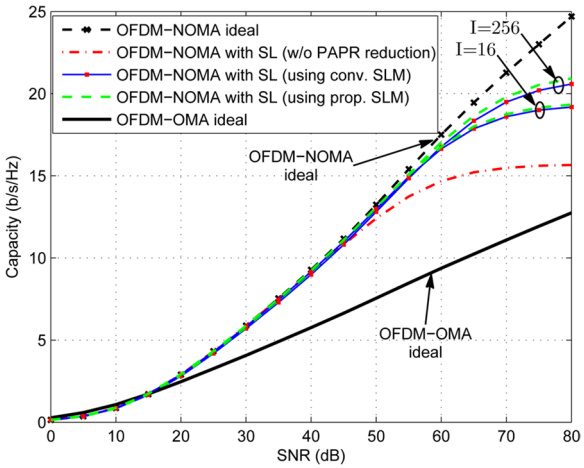

Fig. 6 Sum rate capacity of DL OFDM-NOMA in the presence of nonlinear distortion before and after using conventional and proposed SLM techniques, with different numbers of alternatives $I = 64$ and $I = 256$, compared with the sum rate capacity of DL OFDM-NOMA and DL OFDM-OMA in ideal case

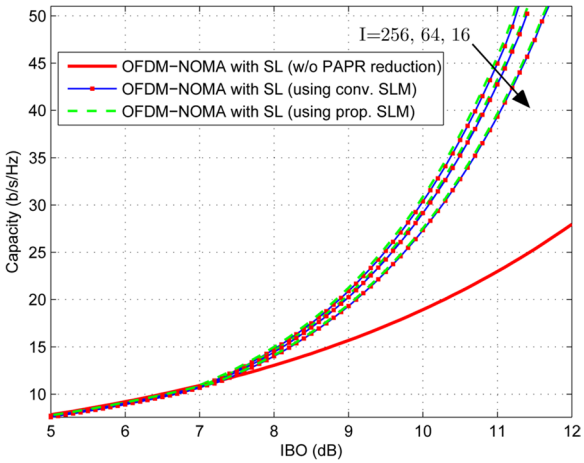

Fig. 7 Asymptotic upper limit of sum rate capacity versus IBO for DL OFDM-NOMA in the presence of nonlinear distortion before and after using conventional and proposed SLM techniques, with different number of alternatives $I = 16$, 64 and 256

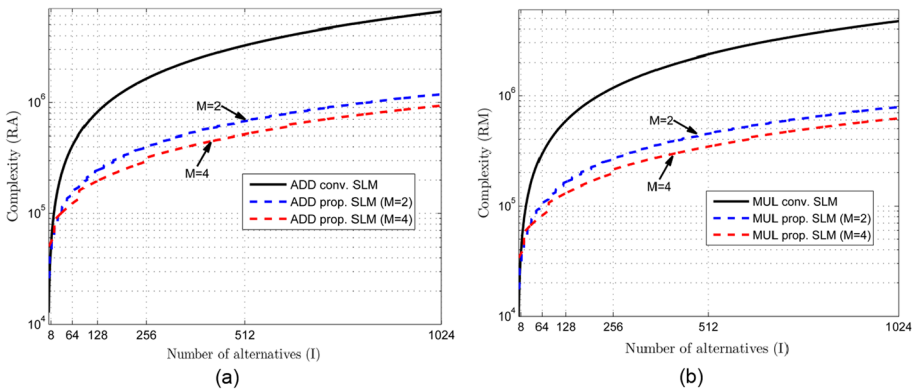

Fig. 8 Comparison of the computational complexity of conventional and proposed SLM techniques, in terms of (**a**) RA and (**b**) RM, for the same number of alternatives in two cases with $M = 2$ and $M = 4$

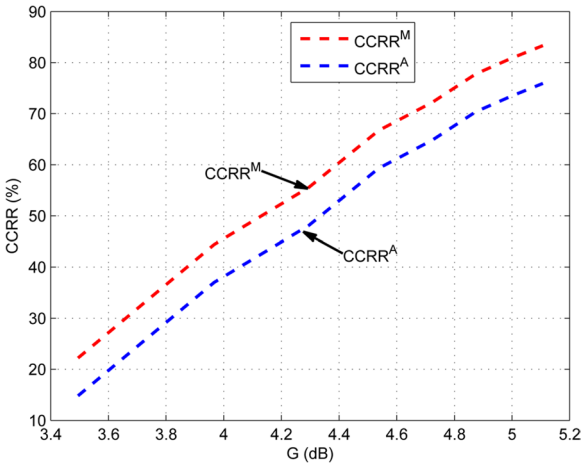

Fig. 9 CCRR of the proposed SLM technique vs. PAPR reduction gain, in terms of RA and RM

increasing the number of users from $M = 2$ to $M = 4$. For example, when the number of alternatives $I = 256$ and the number of users $M = 2$, the proposed SLM technique reduces the required number of RA ($\mathcal{A}_{\text{SLM}}$) and number of RM ($\mathcal{M}_{\text{SLM}}$) by 76% and 78%, respectively. Meanwhile, for $I = 256$ and $M = 4$, the proposed SLM technique reduces the required number of RA ($\mathcal{A}_{\text{SLM}}$) and RM ($\mathcal{M}_{\text{SLM}}$) by 82% and 83%, respectively.

Figure 9 depicts the CCRR of the proposed SLM technique in terms of the number of RA ($\mathcal{A}_{\text{SLM}}$) and RM ($\mathcal{M}_{\text{SLM}}$) versus PAPR reduction gain (G). CCRR is increasing, interestingly, by increasing the PAPR reduction gain (G), i.e., by increasing the number of alternatives (I).

Finally, for the DL OFDM-NOMA system with and without nonlinear distortion, the users' BER is shown in Fig. 10 for different modulation orders. In addition, Fig. 10 depicts users' BER after employing the SLM technique, with a different number of alternatives (I), to mitigate the nonlinear distortion effects. It is not necessary to use the same modulation order NU and FU in the OFDM-NOMA system, as brevity (M2-QAM/M1-QAM) denotes that NU employs M1-QAM modulation, while FU employs M2-QAM modulation. Figure 10 shows three modulation scenarios for NU and FU. The first scenario (4-QAM/4-QAM) is depicted in Fig. 10a and b. In Fig. 10c and d, a second scenario (4-QAM/16-QAM) is shown. The third scenario (4-QAM/64-QAM) is depicted in Fig. 10e and f. For each scenario, different IBO values are used; that is, IBO = 2 dB, 4 dB, and 5 dB are used in the first, second, and third scenarios, respectively.

The BER of the FU in the three scenarios, as shown in Fig. 10a, c, and e, is clearly less affected by the nonlinear distortion than the NU. Furthermore, in the ideal case, FU's BER is independent of NU modulation order, whereas in the presence of nonlinear distortion, FU's BER varies in each scenario due to different IBO values. In addition, Fig. 10a, c, and e shows that the SLM techniques, both conventional and proposed, slightly improve the FU's BER in the presence of the nonlinear distortion, where the degradation in the FU's BER due to the nonlinear distortion is initially small. The SLM

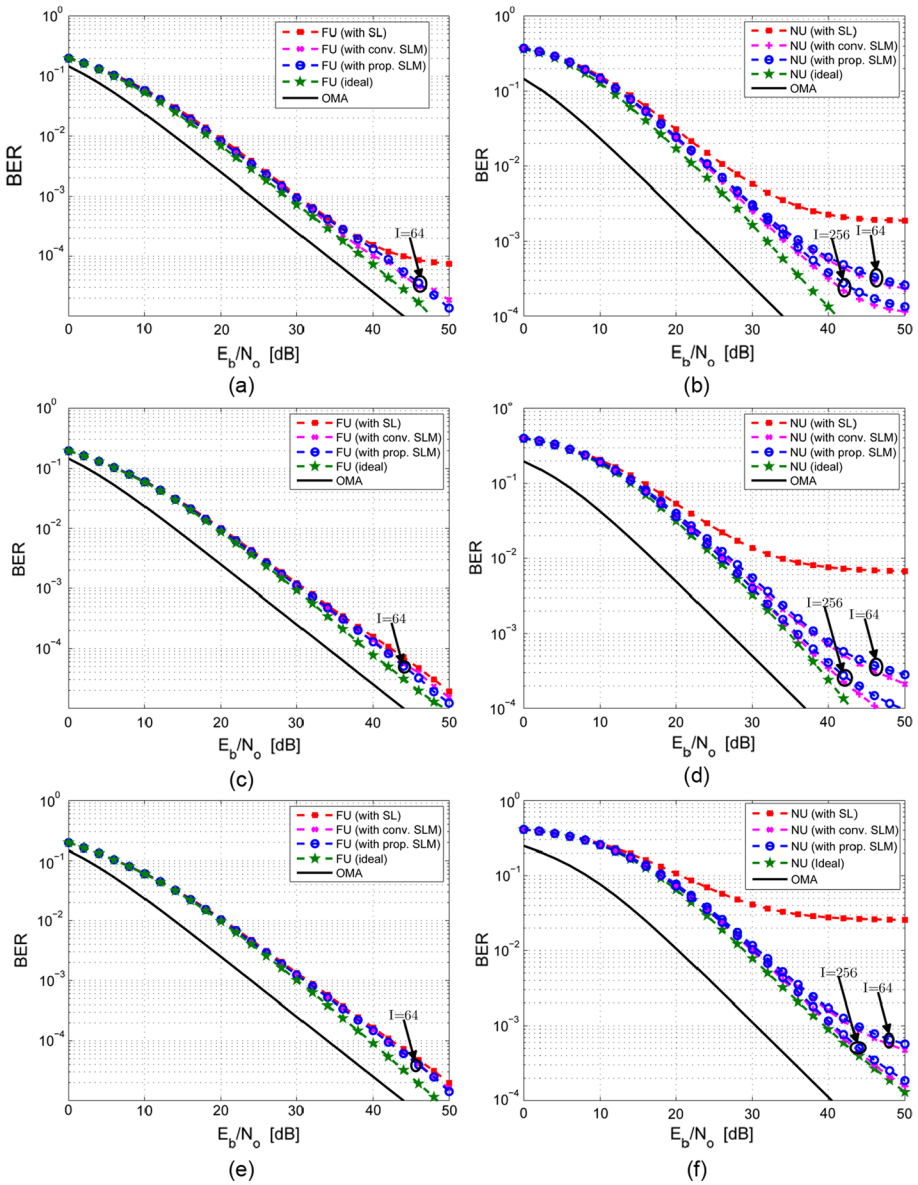

Fig. 10 BER versus E_b/N_o, for both FU and NU, before and after usage of conventional and proposed SLM in the presence of nonlinear distortion for three scenarios. **a** FU in the (4-QAM/4-QAM) scenario, **b** NU in the (4-QAM/4-QAM) scenario, **c** FU in the (4-QAM/16-QAM) scenario, **d** NU in the (4-QAM/16-QAM) scenario, **e** FU in the (4-QAM/64-QAM) scenario, and **f** NU in the (4-QAM/64-QAM) scenario. Ideal NOMA and OMA are shown in all subfigures as a reference. The effect of increasing I from 64 up to 256 on the NU's BER is also investigated in **b**, **d**, and **f**

technique, both conventional and proposed, on the other hand, greatly improves the NU's BER in the presence of nonlinear distortion, as shown in Fig. 10b, d, and f. Furthermore, increasing the number of alternatives (I) of SLM reduces NU's BER in the presence of the nonlinear distortion. It is apparent from Fig. 10b, d, and f that proposed SLM with $I = 256$ at $E_b/N_o = 40$ dB reduces NU's BER from 2.2×10^{-3}, 7.5×10^{-2}, and 2.7×10^{-2} to 3.8×10^{-4}, 4×10^{-4}, and 1.1×10^{-3}, respectively. Furthermore, when

$I = 256$, both proposed and conventional SLM techniques have BER performance comparable to the ideal case. Interestingly, in the case of $I = 256$, the conventional SLM technique requires 1.65×10^6 of RA and 1.2×10^6 of RM, while the proposed SLM technique requires 4×10^5 of RA and 2.6×10^5 of RM. Clearly, the proposed SLM technique reduces the required numbers of RA and RM by 76% and 78%, respectively.

To summarize, the proposed SLM technique, like the conventional SLM technique, improves the performance of the OFDM-NOMA system in the presence of nonlinear distortion, but with a significant reduction in the required computational complexity by utilizing the structure of the OFDM-NOMA transmitter.

7 Conclusion

In conclusion, OFDM-NOMA will be used in 6G to support massive connectivity and high data rate applications. However, OFDM-NOMA, like all multicarrier signals, may suffer from the high PAPR problem, which causes the OFDM-NOMA signal to be distorted after passing through nonlinear HPA. Large IBO values must be used to reduce the effect of nonlinear distortion caused by HPA. Large IBO values, on the other hand, reduce HPA efficiency. As a result, many conventional PAPR reduction techniques were used in the literature to reduce the high PAPR of the OFDM-NOMA signal with different capabilities for each technique. SLM has the highest PAPR reduction gain of these PAPR reduction techniques, but it also has a high computational complexity. In this paper, a novel SLM scheme has been introduced to achieve the same performance as that of the conventional SLM technique while requiring less computational complexity. The proposed SLM technique, as well as the conventional SLM technique, improved the sum rate capacity and user's BER in the presence of nonlinear distortion in the OFDM-NOMA system. Furthermore, the results demonstrated that increasing the number of alternatives and/or users increases the CCRR of the proposed SLM technique.

Author contributions
All authors of this research paper have directly participated in the planning, execution, and analysis of this study; all authors of this paper have read and approved the final version submitted.

Funding
Open access funding provided by The Science, Technology & Innovation Funding Authority (STDF) in cooperation with The Egyptian Knowledge Bank (EKB).

Availability of data and materials
Data sharing is not applicable to this article as no datasets were generated or analyzed during the current study.

Declarations

Ethics approval and consent to participate
Not applicable.

Consent for publication
The contents of this manuscript have not been copyrighted or published previously; the contents of this manuscript are not now under consideration for publication elsewhere; the contents of this manuscript will not be copyrighted, submitted, or published elsewhere, while acceptance by the Journal is under consideration; and there are no directly related manuscripts or abstracts, published or unpublished, by any authors of this paper.

Competing interests
The authors declare that they have no competing interests.

Received: 10 September 2022 Accepted: 22 December 2022
Published online: 16 January 2023

References

1. M. Alsabah, M.A. Naser, B.M. Mahmmod, S.H. Abdulhussain, M.R. Eissa, A. Al-Baidhani, N.K. Noordin, S.M. Sait, K.A. Al-Utaibi, F. Hashim, 6G wireless communications networks: a comprehensive survey. IEEE Access. **9**, 148191–148243 (2021). https://doi.org/10.1109/ACCESS.2021.3124812
2. W. Jiang, B. Han, M.A. Habibi, H.D. Schotten, The road towards 6G: a comprehensive survey. IEEE Open J. Commun. Soc. **2**, 334–366 (2021). https://doi.org/10.1109/OJCOMS.2021.3057679
3. International Telecommunication Union: IMT Traffic estimates for the years 2020 to 2030, https://www.itu.int/pub/R-REP-M.2370-2015, last accessed 2022/04/29
4. Y. Sun, Y. Guo, S. Li, D. Wu, B. Wang, Optimal resource allocation for NOMA-TDMA scheme with α-fairness in industrial internet of things. Sensors **18**, 1572 (2018). https://doi.org/10.3390/s18051572
5. S.M.R. Islam, N. Avazov, O.A. Dobre, K. Kwak, Power-domain non-orthogonal multiple access (NOMA) in 5G systems: potentials and challenges. IEEE Commun. Surv. Tutorials **19**, 721–742 (2017). https://doi.org/10.1109/COMST.2016.2621116
6. Z. Chen, Z. Ding, X. Dai, R. Zhang, An optimization perspective of the superiority of NOMA compared to conventional OMA. IEEE Trans Signal Process. **65**, 5191–5202 (2017). https://doi.org/10.1109/TSP.2017.2725223
7. I. Budhiraja, N. Kumar, S. Tyagi, S. Tanwar, Z. Han, M.J. Piran, D.Y. Suh, A systematic review on NOMA variants for 5G and beyond. IEEE Access **9**, 85573–85644 (2021). https://doi.org/10.1109/ACCESS.2021.3081601
8. M. Mounir, M.B. El Mashade, A.M. Aboshosha, M.I. Youssef, Impact of HPA nonlinearity on the performance of power domain OFDM-NOMA system. Eng. Res. Express **4**, 025004 (2022). https://doi.org/10.1088/2631-8695/AC5AA2
9. F. Ding, H. Wang, S. Zhang, M. Dai, Impact of residual hardware impairments on non-orthogonal multiple access based amplify-and-forward relaying networks. IEEE Access **6**, 15117–15131 (2018). https://doi.org/10.1109/ACCESS.2018.2813081
10. O.B.H. Belkacem, M.L. Ammari, R. Dlnis, Performance analysis of NOMA in 5G systems with HPA nonlinearities. IEEE Access **8**, 158327–158334 (2020). https://doi.org/10.1109/ACCESS.2020.3020372
11. A. Hilario-Tacuri, J. Maldonado, M. Revollo, H. Chambi, Bit error rate analysis of NOMA-OFDM in 5G systems with non-linear HPA with memory. IEEE Access. **9**, 83709–83717 (2021). https://doi.org/10.1109/ACCESS.2021.3087536
12. T. Tang, Y. Mao, G. Hu, A fair power allocation approach to OFDM-based NOMA with consideration of clipping. Electronics **9**, 1743 (2020). https://doi.org/10.3390/ELECTRONICS9101743
13. Z.H. Gebeyehu, Impact of clipping noise on the sum rate of NOMA with PD-DCO-OFDM and conventional DCO-OFDM. Heliyon **6**, e03363 (2020). https://doi.org/10.1016/J.HELIYON.2020.E03363
14. I. Baig, PAPR reduction in 5G cellular networks: a new DCMT precoding based downlink NOMA system. Int. J. Comput. Sci. Inf. Secur. **14**, 1020 (2016)
15. I. Baig, N. ul Hasan, M. Zghaibeh, I.U. Khan, A.S. Saand, A DST precoding based uplink NOMA scheme for PAPR reduction in 5G wireless network, in *2017 7th International Conference on Modeling, Simulation, and Applied Optimization (ICMSAO),* (IEEE, 2017), pp. 1–4. https://doi.org/10.1109/ICMSAO.2017.7934861
16. M.R. Usman, A. Khan, M.A. Usman, S.Y. Shin, Joint non-orthogonal multiple access (NOMA) & Walsh-Hadamard transform: Enhancing the receiver performance. China Commun. **15**, 160–177 (2018). https://doi.org/10.1109/CC.2018.8456460
17. A. Singh, K.K. Naik, C.R.S. Kumar, Impact of SC-FDMA and pilots on PAPR and performance of power domain NOMA-UFMC system, in *International Conference on Ubiquitous and Future Networks, ICUFN*. 2018-July, pp. 507–511 (2018). https://doi.org/10.1109/ICUFN.2018.8436714
18. A. Khan, S.Y. Shin, Linear precoding techniques for OFDM-based NOMA over frequency-selective fading channels. IETE J. Res. **63**, 536–551 (2017). https://doi.org/10.1080/03772063.2017.1299045
19. R. Sayyari, J. Pourrostam, H. Ahmadi, Efficient PAPR reduction scheme for OFDM-NOMA systems based on DSI & precoding methods. Phys. Commun. **47**, 101372 (2021). https://doi.org/10.1016/j.phycom.2021.101372
20. K. Chandekar, D.V. Nithya, Hybrid PAPR reduction using hartley transform pre-coding with clipping and filtering technique in OFDM-NOMA system. Int. J. Electr. Eng. Technol. **11**, 341–348 (2020)
21. I. Baig, U. Farooq, E. Ahmed, M. Imran, M. Shoaib, A hybrid precoding- and filtering-based uplink MC-LNOMA scheme for 5G cellular networks with reduced PAPR. Trans. Emerg. Telecommun. Technol. **29**, e3501 (2018). https://doi.org/10.1002/ETT.3501
22. A. Kumar, A novel hybrid PAPR reduction technique for NOMA and FBMC system and its impact in power amplifiers. IETE J. Res. (2019). https://doi.org/10.1080/03772063.2019.1682692
23. A. Kumar, M. Gupta, A comprehensive study of PAPR reduction techniques: design of DSLM-CT joint reduction technique for advanced waveform. Soft Comput. **24**, 11893–11907 (2020). https://doi.org/10.1007/S00500-020-05086-1
24. D.J.G. Mestdagh, J.L. GulfoMonsalve, J.-M. Brossier, GreenOFDM: a new selected mapping method for OFDM PAPR reduction. Electron. Lett. **54**, 449–450 (2018). https://doi.org/10.1049/el.2017.4743
25. C. Hu, L. Wang, Z. Zhou, A modified SLM Scheme for PAPR Reduction in OFDM Systems, in *ICEIEC 2020 - Proc. 2020 IEEE 10th International Conference on Electronics Information and Emergency Communication*, pp. 61–64 (2020). https://doi.org/10.1109/ICEIEC49280.2020.9152350
26. S.A. Fathy, M. Ibrahim, S. El-Agooz, H. El-Hennawy, Low-complexity SLM PAPR reduction approach for UFMC systems. IEEE Access **8**, 68021–68029 (2020). https://doi.org/10.1109/ACCESS.2020.2982646
27. J.G. Yuan, Q. Shen, J.X. Wang, Y. Wang, J.Z. Lin, Y. Pang, A novel improved SLM scheme of the PAPR reduction technology in CO-OFDM systems. Optoelectron. Lett. **13**, 138–142 (2017). https://doi.org/10.1007/S11801-017-6265-9
28. S. Valluri, V.V. Mani, A novel approach for reducing complexity in the SLM-GFDM system. Phys. Commun. **34**, 188–195 (2019). https://doi.org/10.1016/J.PHYCOM.2019.03.011
29. L. Yang, K.K. Soo, Y.M. Siu, S.Q. Li, A low complexity selected mapping scheme by use of time domain sequence superposition technique for PAPR reduction in OFDM system. IEEE Trans. Broadcast. **54**, 821–824 (2008). https://doi.org/10.1109/TBC.2008.2007451
30. Y. Shirato, M. Muraguchi, Side information-free low computational complexity TDSS-SLM transmission system. ICT Express. **7**, 453–459 (2021). https://doi.org/10.1016/J.ICTE.2021.02.006

31. S.M. Alrabeiy, S.A Fathy, S.M. Gasser, M.S. El-Mahallawy, A modified SLM scheme for PAPR reduction of UFMC systems, in *Journal of Physics: Conference Series*, vol. 2128, p. 012004 (2021). https://doi.org/10.1088/1742-6596/2128/1/012004
32. X. Cheng, D. Liu, W. Shi, Y. Zhao, Y. Li, D. Kong, A novel conversion vector-based low-complexity SLM scheme for PAPR reduction in FBMC/OQAM systems. IEEE Trans. Broadcast. **66**, 656–666 (2020). https://doi.org/10.1109/TBC.2020.2977548
33. C. Gunturu, S. Valluri, A new complexity reduction scheme in selective mapping-based visible light communication direct current-biased optical orthogonal frequency division multiplexing systems. IET Optoelectron. **16**, 207–217 (2022). https://doi.org/10.1049/OTE2.12074
34. P. Jirajaracheep, T. Mata, P. Boonsrimuang, PAPR reduction in FBMC-OQAM systems using trellis-based D-SLM with ABC algorithm, in *17th International Conference on Electrical Engineering/Electronics, Computer, Telecommunications and Information Technology. ECTI-CON 2020,* pp.506–509 (2020). https://doi.org/10.1109/ECTI-CON49241.2020.9158300
35. J. Hou, W. Wang, Y. Zhang, X. Liu, Y. Xie, Multi-Objective quantum inspired evolutionary SLM scheme for PAPR reduction in multi-carrier modulation. IEEE Access. **8**, 26022–26029 (2020). https://doi.org/10.1109/ACCESS.2020.2971633
36. N. Taşpınar, Ş Şimşir, An efficient SLM technique based on migrating birds optimization algorithm with cyclic bit flipping mechanism for PAPR reduction in UFMC waveform. Phys. Commun. **43**, 101225 (2020). https://doi.org/10.1016/J.PHYCOM.2020.101225
37. N. Qamarina, A.A.A. Wahab, W.A.F.W. Othman, S.S.N. Alhady, H. Husin, PAPR reduction of OFDM system using selective mapping (SLM) and firefly algorithm (FA). Lect. Notes Electr. Eng. **770**, 255–271 (2022). https://doi.org/10.1007/978-981-16-2406-3_20
38. M. Mounir, M.B. El-Mashade, A. Mohamed Aboshosha, On the selection of power allocation strategy in power domain non-orthogonal multiple access (PD-NOMA) for 6G and beyond. Trans. Emerg. Telecommun. Technol. **33**, e4289 (2022). https://doi.org/10.1002/ett.4289
39. Z. Ding, Z. Yang, P. Fan, H.V. Poor, On the performance of non-orthogonal multiple access in 5G systems with randomly deployed users. IEEE Signal Process. Lett. **21**, 1501–1505 (2014). https://doi.org/10.1109/LSP.2014.2343971
40. Y. Rahmatallah, S. Mohan, Peak-to-average power ratio reduction in ofdm systems: a survey and taxonomy. IEEE Commun. Surv. Tutorials. **15**, 1567–1592 (2013). https://doi.org/10.1109/SURV.2013.021313.00164
41. F. Sandoval, G. Poitau, F. Gagnon, Hybrid peak-to-average power ratio reduction techniques: review and performance comparison. IEEE Access. **5**, 27145–27161 (2017). https://doi.org/10.1109/ACCESS.2017.2775859
42. J.G. Andrews, A. Ghosh, R. Muhamed, *Fundamentals of WiMAX: Understanding Broadband Wireless Networking* (Pearson Education, Prentice Hall, Upper Saddle River, NJ, United States, 2007)
43. H.Y. Liang, Modified selective mapping based on squaring construction. Int. J. Commun. Syst. **35**, e5029 (2022). https://doi.org/10.1002/DAC.5029
44. R.F.H. Fischer, M. Hoch, Peak-to-average power ratio reduction in MIMO OFDM, in 2007 IEEE International Conference on Communications, (IEEE, 2007), pp. 762–767. https://doi.org/10.1109/ICC.2007.130
45. S. Thota, Y. Kamatham, C.S. Paidimarry, Analysis of hybrid PAPR reduction methods of OFDM signal for HPA models in wireless communications. IEEE Access. **8**, 22780–22791 (2020). https://doi.org/10.1109/ACCESS.2020.2970022
46. M. Mounir, M.B. El-Mashade, G.S. Gaba, On the selection of the best MSR PAPR reduction technique for OFDM based systems. Lect. Notes Networks Syst. **114**, 157–173 (2020). https://doi.org/10.1007/978-981-15-3075-3_11
47. L. Yang, W. Hu, K. Soo, Y. Siu, Swapped SLM scheme for reducing PAPR of OFDM systems. Electron. Lett. **50**, 1608–1609 (2014). https://doi.org/10.1049/el.2014.1310

Publisher's Note